Numerical and Experimental Comparison of Spinnaker Aerodynamics Close to Curling

Benoit Augier, Benoit Paillard, Matthieu Sacher, Jean-Baptiste Leroux, Nicolas Aubin

Journal of Sailing Technology 2021, volume 6, issue 1, pp. 118 – 132.
The Society of Naval Architects and Marine Engineers.

Numerical and Experimental Comparison of Spinnaker Aerodynamics Close to Curling.

Benoît Augier
IFREMER, Brest Deep Wave Tank, France, benoit.augier@ifremer.fr

Benoît Paillard
Alternative Current Energy, France

Matthieu Sacher
ENSTA Bretagne, CNRS UMR 6027, IRDL, France

Jean-Baptiste Leroux
ENSTA Bretagne, CNRS UMR 6027, IRDL, France

Nicolas Aubin
Doyle Sails, New Zealand

Manuscript received December 4, 2021; revision received June 2, 2021; accepted June 21, 2021.

Abstract. When sailing downwind with a spinnaker, the "verge of curling" is one of the common recommendations that sailors follow for efficient sailing. Wind tunnel experiments on spinnaker models conducted by Aubin et al. (2017) in the Twisted Flow Wind Tunnel of the Yacht Research Unit of the University of Auckland have shown that curling can be related to better performance at Apparent Wind Angle ≥ 100°. In the present article, we will focus on the aerodynamic performance jump observed at Apparent Wind Angle AWA = 100°, where the drive force increases up to 15% when the sail starts to flap. Thanks to four triggered HD cameras and coded targets stuck on the sail, three flying shapes of the spinnaker are reconstructed by photogrammetry for different sheet lengths from over trimmed to flapping occurrence. The pimpleFOAM solver from OpenFOAM is used to simulate the aerodynamics of the three rigid extracted flying shapes. Results highlight the ability of the model to simulate the experimental jump observed closed to curling and the significant confinement effect of the roof of the wind tunnel.

Keywords: CFD; Spinnaker; RANS; NE comparison.

NOMENCLATURE

C_{Fx}	Drive force coefficient
C_{Fy}	Side force coefficient
L_{sheet}	Sheet length
U_x	Flow velocity in the x direction [m.s^{-1}]
AWA	Apparent Wind Angle [°]
CFD	Computational Fluid Dynamics
URANSE	Unsteady Reynolds Average Navier-Stokes Equation

1. INTRODUCTION

The “verge of curling” recommendation is one of the most common pieces of advice that sailors follow for efficient sailing downwind with a spinnaker. Full-scale tests, thanks to the VOILENav project and the Sailing Fluids program, have recently investigated this complex unsteady Fluid-Structure Interaction phenomenon based on pressures and flying shape measurements (Motta et al. 2014, Deparday, 2016, Deparday et al., 2018). These results showed that the curling of the leading edge of the spinnaker was associated with a pressure field evolution (Deparday et al. 2017), whose propagation generates high suction peaks on the luff area. Arredondo and Viola (2016) studied a similar behavior with the Leading-Edge Vortex (LEV) flow pattern. Souppez et al. have reviewed the experimental and numerical approaches on downwind sails (Souppez et al., 2019). In a recent study Aubin et al. (2017), wind tunnel experiments on a spinnaker were conducted in the Twisted Flow Wind Tunnel (TWFT) (Flay, 1996) of the Yacht Research Unit of the University of Auckland measuring simultaneously aerodynamic forces, sheet length, sheet load, and flying shape recorded by four triggered HD cameras (Fig. 1). Aubin et al. (2017) showed that curling can be related to better performance at Apparent Wind Angle ≥ 100°.

In the present article, we will focus on the aerodynamic performance jump observed at AWA = 100° (Fig. 2), where the drive force increases up to 15% just before the sail starts to flap. The question asked here is: **can we simulate this observed increase?**

To better assess the aerodynamic performance of downwind sails, Viola (2009) and Viola et al. (2014) have numerically provided insights into the flow behavior, in particular in the luff area. Numerical simulations have also been performed on a fixed sail shape validated with wind tunnel experiments on flexible (Viola et al., 2009, 2013, 2015) and semi-rigid sails (Bot et al. 2013, 2014). Nonetheless, the realistic fluid-structure interaction simulations of downwind sails represent a significant step forward.

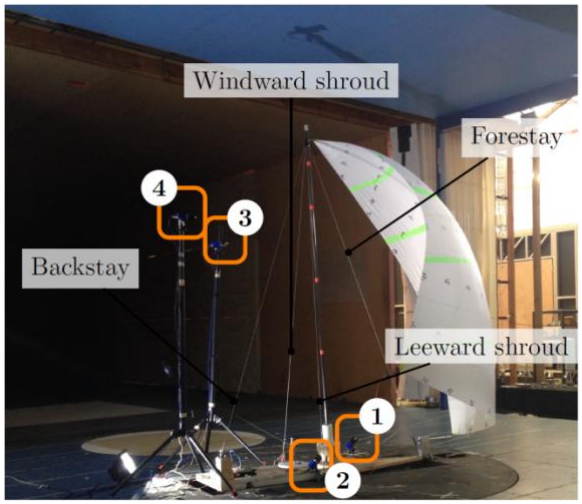

Figure 1: Experimental set up in the TFWT, Auckland, to measure the aerodynamic loads and spinnaker flying shape. The orange squares highlight the 4-photogrammetry cameras.

The added complexity is in considering the significant influence of the added mass and simulating the curling of the luff, which is challenging mostly due to substantial displacements of the sail, requiring specific and complex mesh deformation methods. As a first approach, a finite element method has been coupled to a flow solver (Renzsch et al., 2013, 2016;Trimarchi et al., 2013) to predict the sail flying shape in static simulations. Lombardi et al. (2012), Durand (2012) and Durand et al. (2010, 2014) successfully achieved unsteady fluid-structure interaction simulations. Still, so far, such simulations have not been compared to full-scale or wind tunnel experimental unsteady data, such as the dynamic curling behaviour at a fixed trim.

The problem is simplified here by considering 3 rigid flying shapes of the spinnaker reconstructed by photogrammetry (Deparday, 2016) for different sheet lengths from over-trimmed to flapping occurrence.

Unsteady RANSE simulations using the pimpleFOAM solver from OpenFOAM are achieved on these rigid geometries and compared with experimental results. Authors believe that URANSE can simulate the aerodynamics of spinnakers with an appropriate mesh, contrarily to previous studies (Lasher et al., 2008, Nava et al., 2017) where the simulations underestimated the aerodynamic loads.

The first part of the paper describes the wind tunnel experimental set up and the flying shape recovery. The URANSE numerical model is then presented together with the meshing characteristics. Simulation results are eventually compared to the experiment looking at the sensitivity of confinement and apparent wind angle.

2 EXPERIMENTAL APPARATUS

The presented experimental apparatus is part of a more extensive set up described in detail in (Aubin, 2017, Aubin et al. 2017). Here, the purpose of the set-up is to link the aerodynamic performances to the so-called “flying shape” for different sail trims.

2.1 Driving force measurement

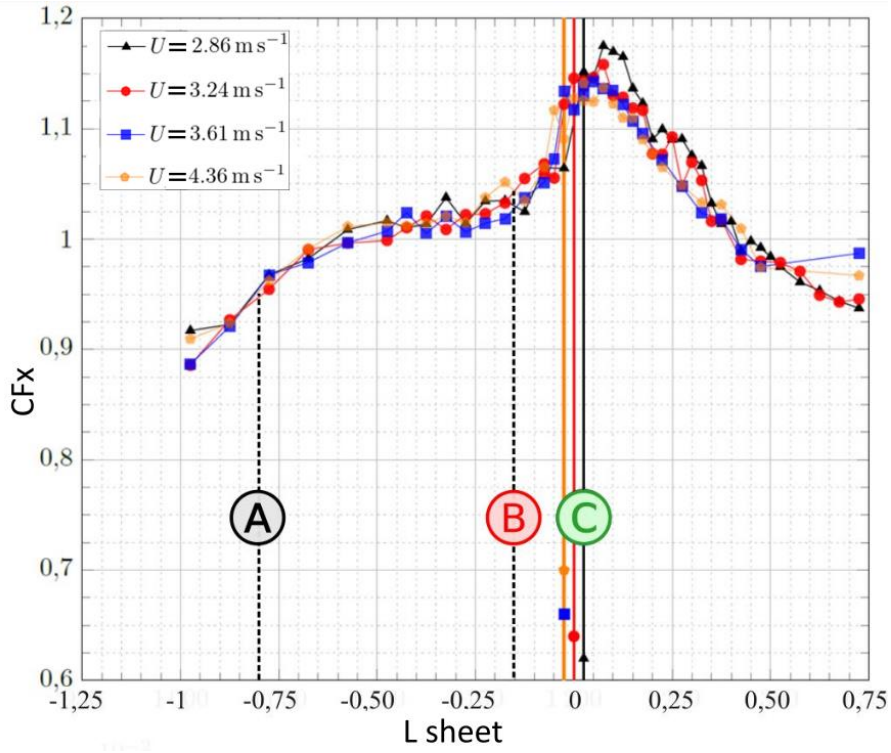

Figure 2: Evolution of driving force coefficient with the sheet length measured in the TFWT at AWA = 100° and 4 wind speeds (Aubin et al., 2017). A, B, and C refer to the 3 studied cases. Solid vertical lines represent flapping occurrence. Lsheet < 0 corresponds to over trimmed cases.

A 6 DoF dynamometer attached to the floor and connected to the model measures the forces. The AWA is modified with a turning table, levelled with the floor. The balance turns with the table, linking then the measurement axis with the model axis. The balance measures the forces into the upright boat frame referential, so it measures directly the drive (along x-axis) and side force (along y-axis). The balance can be seen on Figure 3. (Hansen 2006) provides information about the force balance error: ±0.09 N along x direction, ±0.11 N along y direction and ±0.27 N along z direction. For typical parameter values measured during the experimental campaign, we get an uncertainty of ±0.05 on CFx, ±0.06 on CFy and ±0.08 on CFz. The velocity measurement error with the Pitot Tube is about 1%.

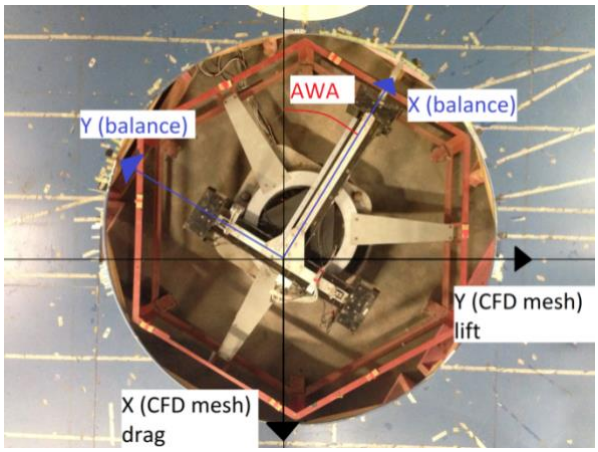

Figure 3: Bird eye's view on the force balance. The hexagonal support frame rotates the force balance to modify the apparent wind angle. (a) is taken when the balance x axis is aligned with the incoming flow (Aubin, 2017).

The balance is supported by a rotating orange hexagonal frame, which allows adjusting the apparent wind angle noted AWA. The CFD drive and side force coefficients can be obtained from the lift C_L and drag C_D coefficients, respectively along the Y and X domain mesh referential axis thanks to the formula:

$$C_{FX} = -C_D \cos(AWA) + C_L \sin(AWA)$$
$$C_{FY} = -C_D \sin(AWA) - C_L \cos(AWA)$$

The driving force coefficient is defined as the normalized force in the forward longitudinal axis of the boat when the side force coefficient is in the lateral axis (portside).
At fixed AWA, the sheet length has a significant effect on the driving force (Fig. 2). When easing the sheet, the driving force increases until reaching a maximum at the verge of curling. Coloured vertical lines in Figure 2 indicate curling appearance. It is important to notice that the driving force jump is observed for all studied wind speed and spinnakers.

2.2 Flying shape measurements

2.2.1 Photogrammetry set up

The flying shape of the spinnaker is significantly impacted by the sail trimming, even with a constant AWA. The geometry of the sail is extracted by means of the photogrammetry technique using the Photomodeler Software. Four HD cameras - with locations as shown in Fig. 1 - record 2046 x 2046 black and white photographs at 20fps. Cameras are synchronized with the load balance. A total of 51 coded targets are stuck on the sail (Fig. 4), dividing the sail into 7 lines. Markers are also stuck in the wind tunnel walls and ceiling as a coordinate system and scale reference. The positions of the markers are extracted using Photomodeler software (Fig. 4) and exported to Rhinoceros 3D to build a surface.

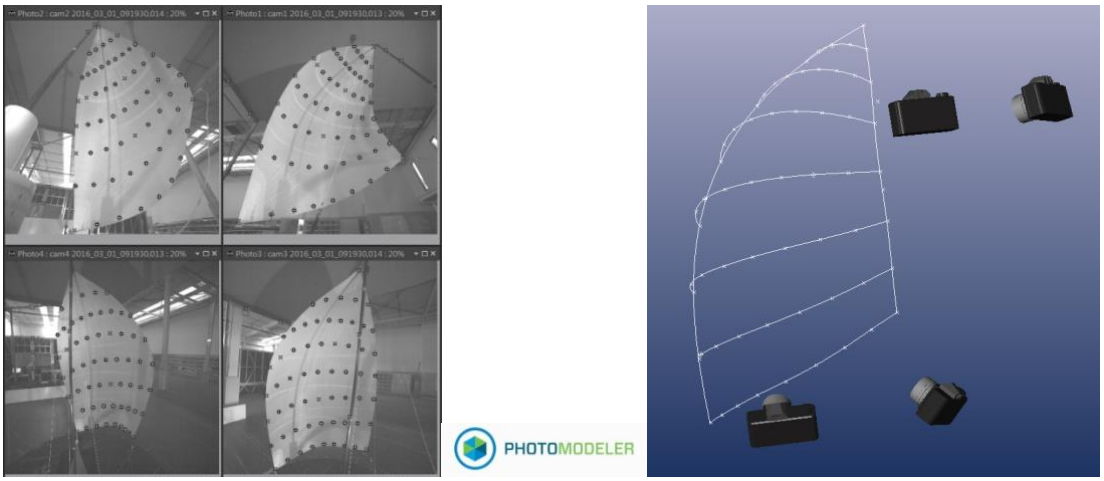

Figure 4: Flying shape reconstruction by photogrammetry with Photomodeler software.

The dynamic behavior of a spinnaker comes from a coupled FSI problem. The present work aims to model flow instabilities and possible flow separations, on non-deformable spinnaker geometries at several fixed sheet lengths. For each sheet length, one spinnaker geometry is extracted from the experiments by using the median flying shape. In other words, the extracted geometries at each sheet length are static representations of dynamic spinnaker behaviors. This hypothesis is good for over trimmed sails but starts to be questionable close to curling where the sail moves.

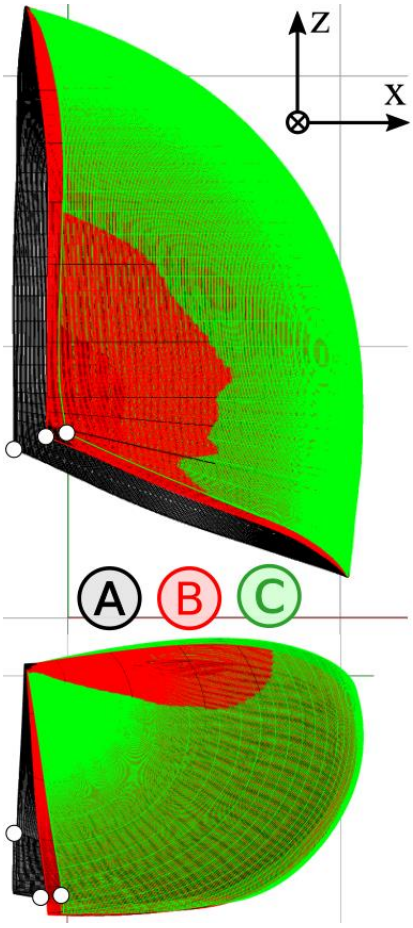

Figure 5: Comparison of the 3 extracted flying shapes. The sheeting point are represented by a white circle.

2.2.2 Definition of the studied cases

Three different cases are defined for the study. The cases are chosen to represent the full range of aerodynamic performance of the spinnaker (Fig. 2). Sheet lengths are dimensionless from over trimmed -1, the mechanical limit of the trimming system, to the verge of curling 0:

A. L_{sheet} = -0.8 → Spinnaker over trimmed
B. L_{sheet} = -0.15 → End of low CFx variation
C. L_{sheet} = 0 → On the verge of curling

As illustrated in Figure 5, the sheeting point moves forward and upward when easing the sail, when the luff is sliding windward. The 3 geometries are exported in .stl files as thick surfaces (1mm thickness) for the simulations. Geometries are available online (see references)

3 NUMERICAL MODELS

3.1 OpenFOAM

The parallel incompressible viscous flow solver OpenFOAM is used to solve the Unsteady Reynolds-Average Navier-Stokes Equations (URANSE). The pressure-velocity coupling is achieved with a SIMPLE algorithm, and the standard two equations shear stress transport (SST) model (Menter et al., 2003) is presently used for turbulence modelling. The choice of turbulence model is motivated by the fact that the k-ω SST model is widely used in CFD, and that it has not yet been shown that another turbulence model is clearly more accurate today (Lasher et al., 2008, Wang et al. 2017).

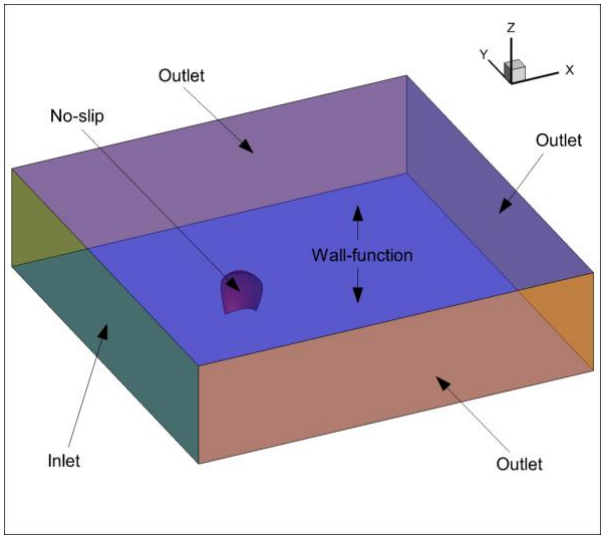

Figure 6: Computational domain with boundary conditions (domain is not to scale).

A parallelepiped computational domain enclosing the spinnaker is considered with extensions [-20 m, 80 m] x [-10 m, 10 m] x [0 m, 3.5 m] in X, Y and Z directions respectively. This domain is illustrated in Figure 6, where boundary conditions that are applied to the different domain faces are also provided. In particular, a uniform velocity of 3.25 m/s aligned with the X-axis is prescribed at the inlet plane. At the top and bottom planes, wall-function boundary conditions are used to model the roof and floor of the wind tunnel. Spinnaker surfaces are no-slip boundary conditions, and at the remaining outlet planes, the pressure is prescribed to zero.

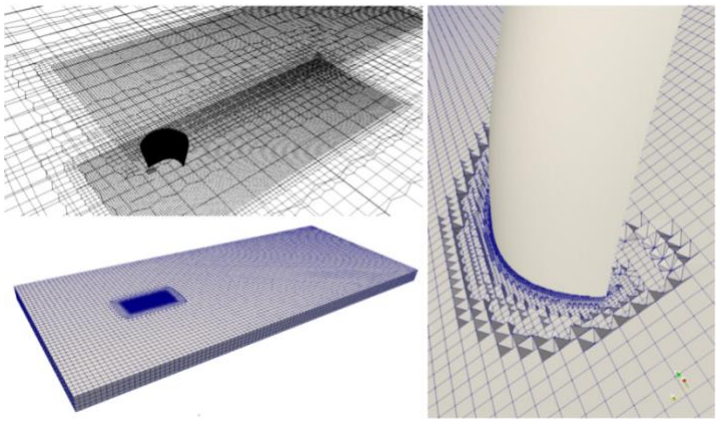

Figure 7: Unstructured mesh of the domain and refinement box around the spinnaker. Mesh refinement around the sail highlighting the boundary layers.

The fluid domain is meshed using the unstructured automatic mesh generator Cf-Mesh. The meshed domain is built with hexahedral cells (Fig. 6 - 7), except in regions close to spinnaker edges where prismatic cells are generated to allow an accurate boundary layer modelling. First cell thicknesses of domain regions with wall-type boundary conditions (Knopp et al., 2006, Fangingg 2016) are set according to y+ criteria. Individually, it has been considered a y+ value of 80 for wall function boundary conditions. For no-slip boundary conditions on spinnaker surfaces, a value of y+ < 5 is ensured on the whole surface, leading to first layer thicknesses of about 0.7 mm. This y+ value is determined after a convergence study and ensures to keep the mesh size and quality at the optimal value. A mesh refinement box with a target cell size of 50 mm and extensions [-1.2 m, 6 m] x [-1.2 m, 2.5 m] x [0 m, 3 m] in X, Y and Z directions respectively, is also set in order to capture better spinnaker wake flows. The total number of cells is about 13 million, and the computing time on a high-performance cluster using 64 CPUs is about 1 CPUh per second. Results presented in this paper are time averaged over 1 second, after roughly 10 seconds of computation. In the following, time variations of results are not shown as values are very low. Mesh convergence study is presented in Figure 8. The impact of the number of cells on the propulsive force and the pressure distribution is illustrated. The low-pressure magnitude and area near the leading-edge increase with the number of cells. The contribution of this suction area is significant on the propulsive force.

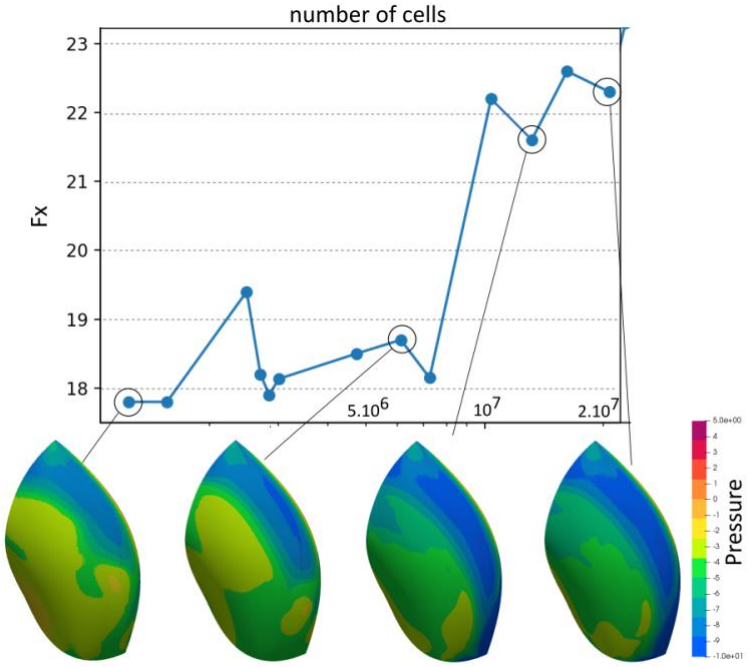

Figure 8: Impact of mesh refinement on propulsive force Fx and pressure distribution (1.2M, 6M, 13M and 20M cells).

4 RESULTS

Previous numerical studies made on the TFWT (Nava et al., 2017) have chosen a detailed modelling of the tunnel inlet condition. In this study, we only focus on two geometrical parameters: the AWA and the effect of the roof. These parameters have, from the authors' experiences in Auckland's wind tunnel, the most significant effect on the results. Sensitivity with AWA is first investigated. The effect of Z confinement is then studied.

4.1 Sensitivity to AWA

In the TFWT, a turning table helps to set the AWA (Flay, 1996). This angle setting is very sensitive to the users and could significantly differ from a campaign to another by ±5°. Indeed, the AWA setting is not digitalized in the TFWT, leading to a hand user setting with markers. This precision is then considered in the simulations where different AWA are computed, from 100° to 93° for the case C. The sensitivity of aerodynamic coefficients to AWA is then studied. Figure 9 represents the evolution of the driving coefficient CFx with the different apparent angles for the case C, close to curling. The case C is the most sensitive to the apparent angle.

The aerodynamic forces are very sensitive to the AWA. As illustrated in Figure 9, The forces increase slowly as the angle decrease before getting to a peak around 95° (relatively -5° from the reference angle AWA=100°). For angle < 95°, the force continues to increase, following the same slow trend observed for the first steps. The effect of the AWA is also illustrated in the pressure distribution map where the suction zone progressively extends in the LE area. These results highlighted the sensitivity of the AoA and confirm the existence of an experimental offset in the data. Despite the precision of the absolute reference of the angle, the turning table set up is repeatable. We then apply a correction of -5° in all the computation, bringing the reference 100° to 95°.

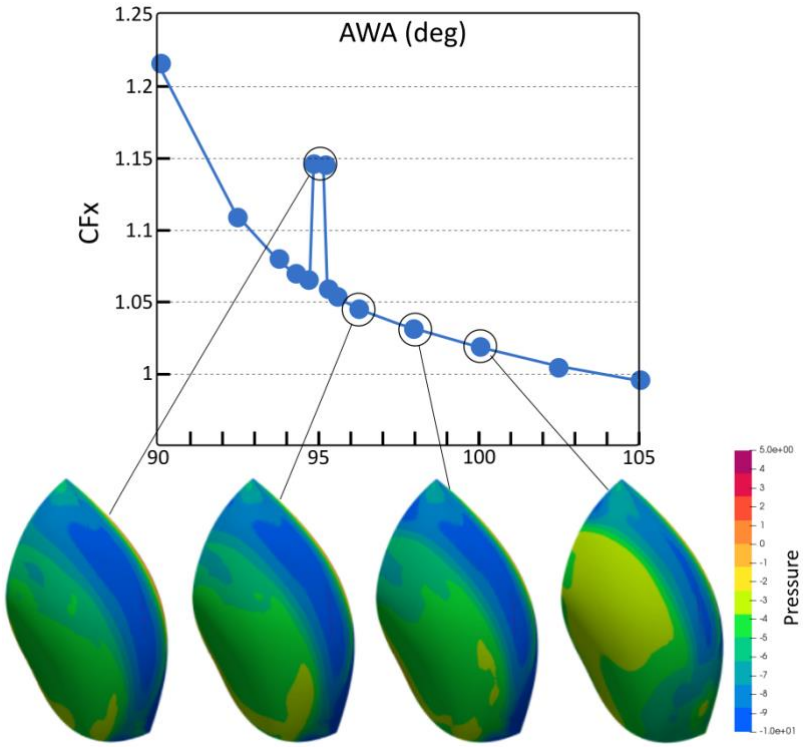

Figure 9: Evolution of the propulsive force coefficient with the apparent wind angle AWA.

4.2 Sensitivity to Z confinement

In the TFWT test section, the only remaining walls are the floor and the roof. The foot of the sail is at 0.15m of the deck, and the floor is simulated. The influence of the roof on the aerodynamic performance is studied to quantify the confinement effects of the tunnel, the sail's head is at 2.37m when the testing section height is Z = 3.5m. As illustrated in Figures 10 and 11, considering the roof affects the results, increasing the aerodynamic coefficients. Several quantities are presented in the following analysis to understand the effect of trim on the aerodynamics.

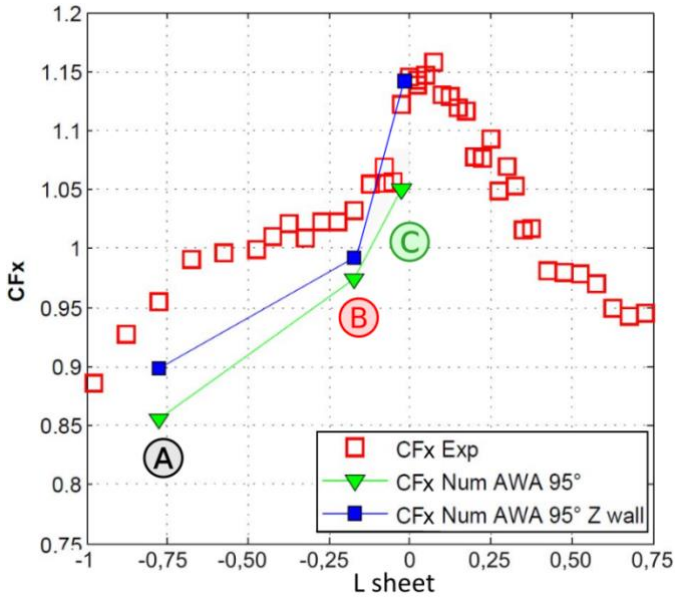

Figure 10: CFx as a function of the trim using a wall-function condition on the top domain plane.

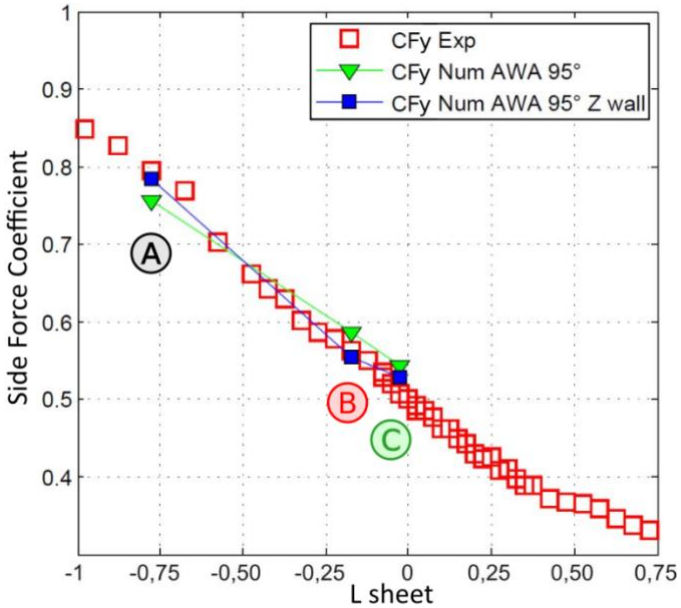

Figure 11: -CFy as a function of the trim using a wall-function condition on the top domain plane.

4.2.1 Pressures on the field

Normalised pressure ρ is plotted for the different flying shapes in the YX plane (Z=1.85m) in Figure 12 and the ZX plane in Figures 13 and 14 respectively, with and without confinement. First, the ZX representation illustrates the importance of the confinement effect due to the modelling of a wall at the roof. The over speeds observed up to the roof in the confinement case are limited to the really top of the sail in the outlet case. Second, the trim has an important effect on the downstream domain. When easing the sail, the low-speed area downstream of the spinnaker decreases and condenses to the bottom part. Eventually, streamlines of the eased case C are more aligned with the upstream flow, when case A seems to be subject to more significant and stronger turbulent structures.

In the YX plane, the evolution of the suction peak is clearly visible in the domain with an important low-pressure area near the leading edge, getting more prominent when the sail is eased.

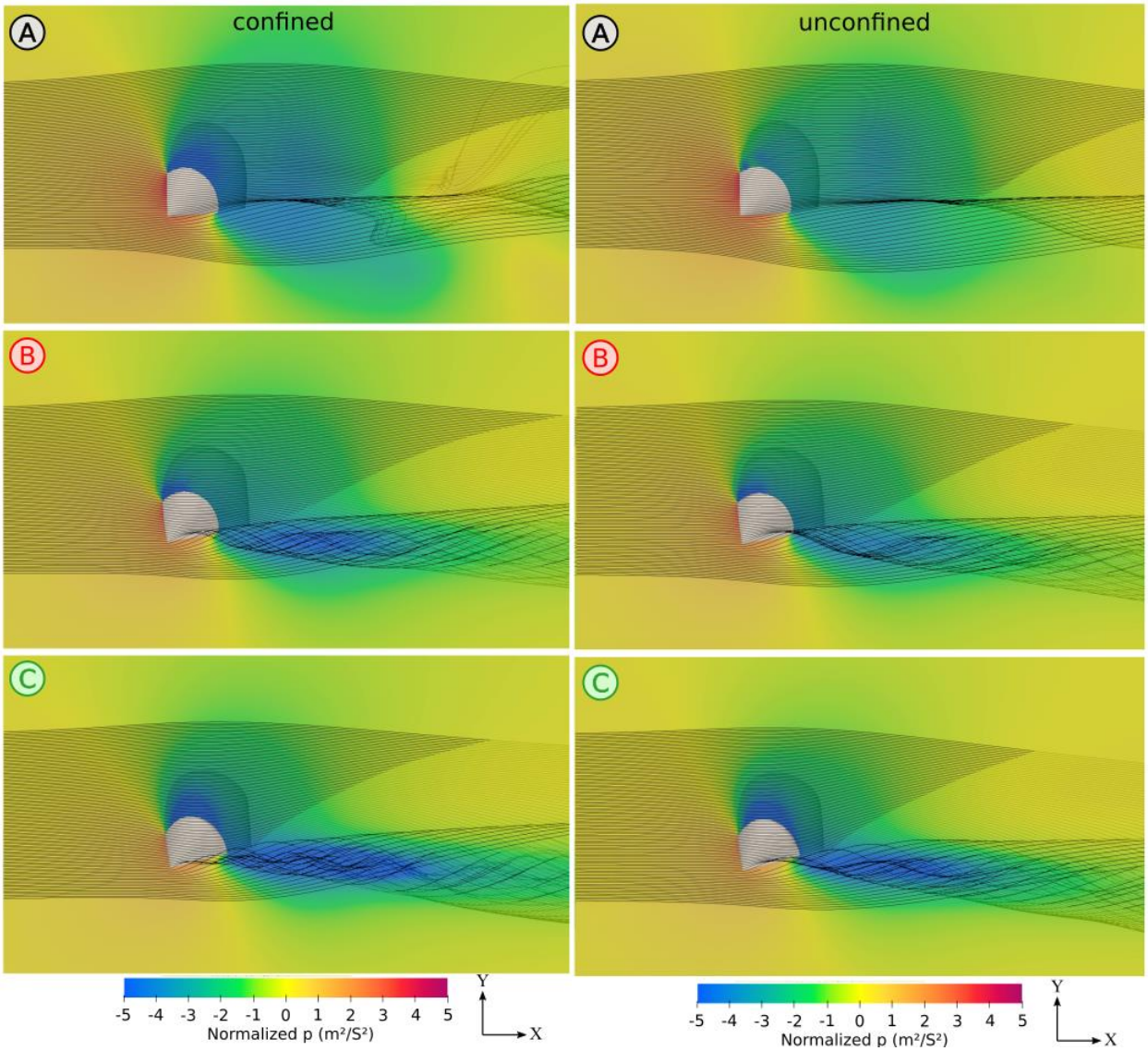

Figure 12: Normalized pressure in the plan Z=1.85 for the different trimming using a wall-function condition "confined" or an outlet condition "unconfined" on the top domain plane (OpenFOAM URANSE – k-ω SST).

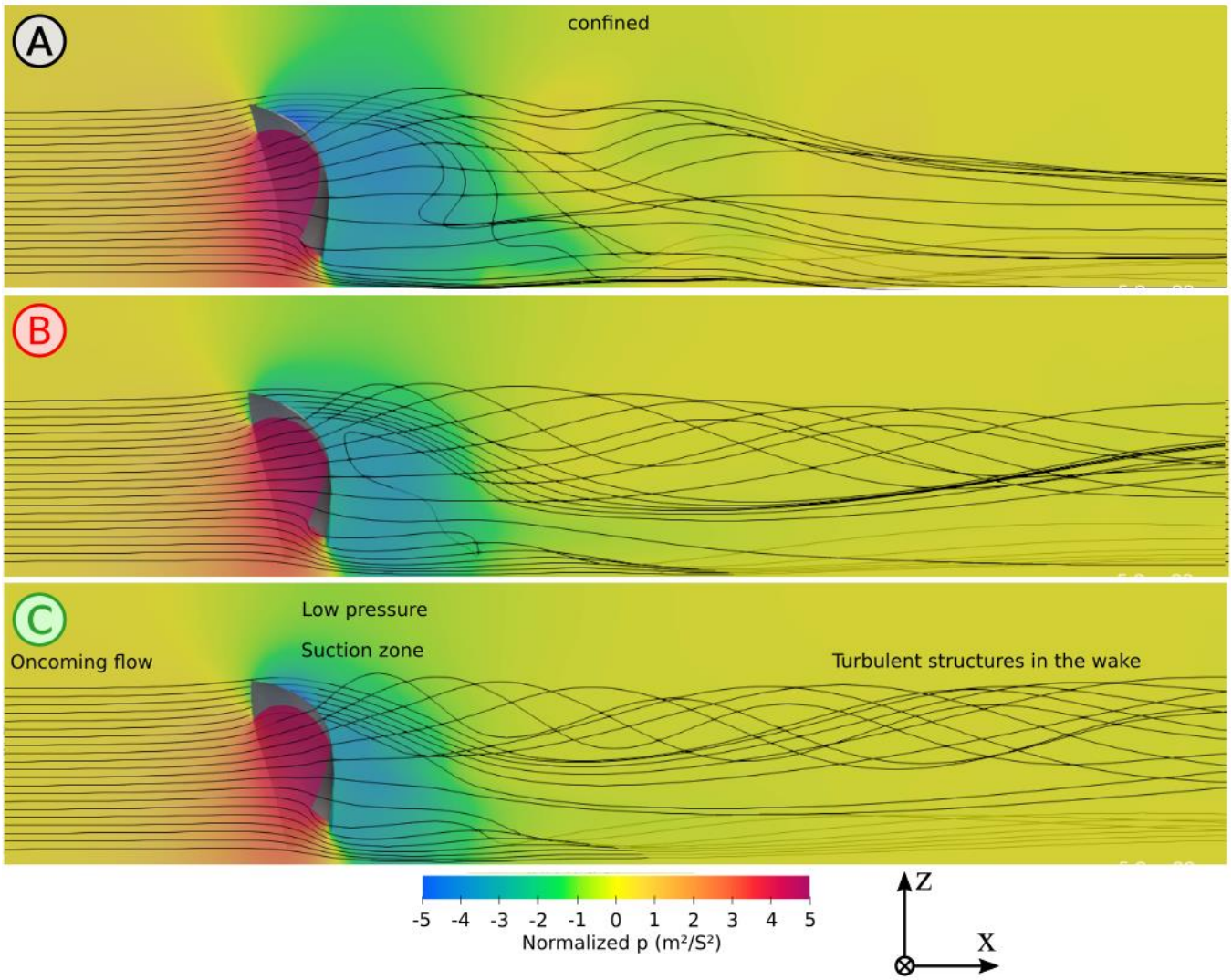

Figure 13: Normalized pressure for different spinnaker trimming using a wall-function condition on the top domain plane (OpenFOAM URANSE – k-ω SST).

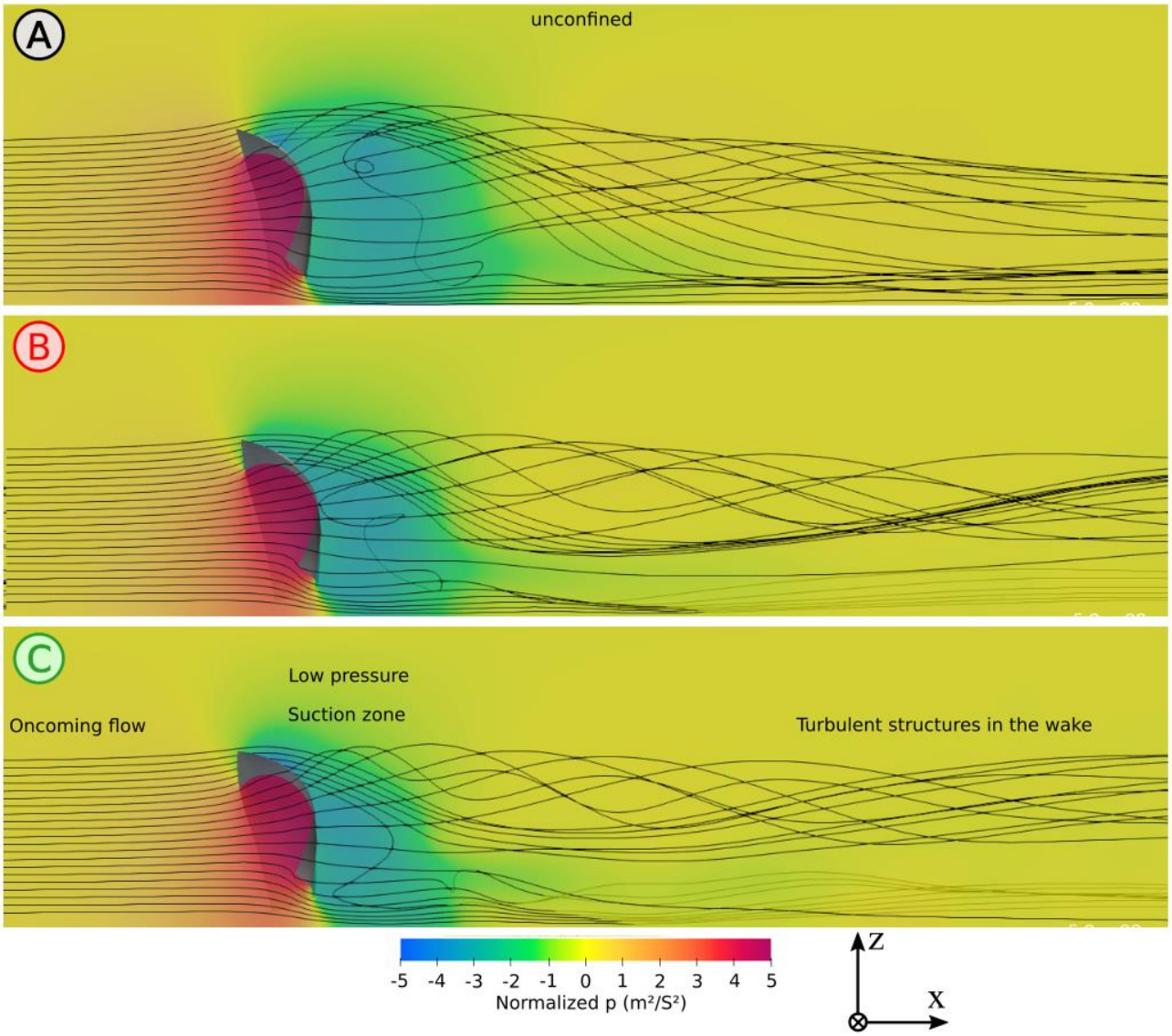

Figure 14: Normalized pressure for different spinnaker trimming using a pressure outlet condition on the top domain plane (OpenFOAM URANSE – k-ω SST).

5 CONCLUSIONS

In this article, a numerical model has been set up to compute URANSE simulation of spinnakers for different trimming. These simulations are compared to experimental data measured in wind tunnel where a jump was observed on the verge of curling. The results of numerical and experimental comparisons can be summarised in four points:

- A URANSE approach based on pimpleFOAM solver from OpenFOAM is able to simulate the aerodynamic performance of a spinnaker correctly and to compute the observed drive force jump close to curling.
- The AWA has a strong influence on the simulation results, especially on drive force jump modelling.
- The confinement effect has a limited effect on the global pressure distribution but influences greatly the magnitude of the suction peak located at the top of the sail.
- On the verge of curling, the suction peak moves from the leading edge to the centre of the sail, creating a relatively high pressure that extends over the curling part.

Further work will concern a focused study on considering the walls of the wind tunnel at the computation domain velocity inlet plane (Viola et al., 2013, Nava et al., 2017). URANSE-LES computations may also be conducted in future works.

ACKNOWLEDGEMENTS

The experimental work presented was supported by Brest Métropôle Océane, the French Naval academy, and has received fundings from the European Union's Seventh Program SAILING FLUIDS, noPIRSES-GA-2012-318924.

REFERENCES

A. Arredondo and I. M. Viola (2016). On the leading edge vortex of thin wings. In 69th Annual meeting of the APS Division of Fluid Dynamics Meeting Abstracts, volume 61, Portland, Oregon, USA.

N. Aubin, B. Augier, J. Deparday, and M. Sacher (2017). To curl or not to curl: wind tunnel investigation of spinnaker performance. *In Conference on Innovation in High Performance Sailing Yachts INNOVSAIL 2017*, Lorient, France.

N. Aubin, (2017) Fluid-structure interaction on yacht sails: from full-scale approach to wind tunnel unsteady study. *PhD Thesis.*

P. Bot, I. M. Viola, R. G. J. Flay, and J.-s. Brett (2013). Wind Tunnel pressure measurements on model-scale semi rigid downwind sails. In The Third International Conferenceon Innovation in High Performance Sailing Yachts (Innovsail), pages 119–127, Lorient, France.

P. Bot, I. M. Viola, R. G. J. Flay, and J.-S. Brett (2014). Wind Tunnel pressure measurements on model-scale rigid downwind sails. Ocean Engineering, 90:84–92.

J. Deparday (2016). Experimental studies of Fluid-Structure Interaction on Downwind Sails. PhD thesis, Université de Bretagne Occidentale, Brest.

J. Deparday, B. Augier, P. Bot (2018). Experimental analysis of a strong fluid–structure interaction on a soft membrane—Application to the flapping of a yacht downwind sail. Journal Of Fluids And Structures, 81, 547-564.

J. Deparday, P. Bot, F. Hauville, B., Augier, M., Rabaud, D., Motta, D., Le Pelley (2017). Modal analysis of pressures on a Full-Scale Spinnaker. Journal of Sailing Technology 2 (01): 1–21.

M. Durand, F. Hauville, P. Bot, B. Augier, Y. Roux, A. Leroyer, and M. Visonneau (2010). Unsteady numerical simulationsof downwind sails. In International Conference on Innovation in High Performance Sailing Yachts, Lorient, France.

M. Durand (2012). Interaction fluide-structure souple et légère, applications aux voiliers. PhD thesis, Ecole Centrale de Nantes.

M. Durand, A. Leroyer, C. Lothodé, F. Hauville, M. Visonneau, R. Floch, and L. Guillaume (2014). FSI investigation on stability of downwind sails with an automatic dynamic trimming. Ocean Engineering, 90:129–139.

R. G. J. Flay (1996). A twisted flow wind tunnel for testing yacht sails. Journal of Wind Engineering and Industrial Aerodynamics, 63(1-3):171–182.

H. Hansen (2006). Enhanced Wind Tunnel Techniques and Aerodynamic Force Model for Yacht Sails, PhD Thesis.

T. Knopp, T. Alrutz and D. Schwamborn (2006). A grid and flow adaptive wall-function method for RANS turbulence modelling. Journal of Computational Physics, 220(1), 19-40.

Liu, Fangqing. "A thorough description of how wall functions are implemented in OpenFOAM." *Proceedings of CFD with OpenSource software* (2016): 1-33.

W.C. Lasher, J.R. Sonnenmeier (2008). An Analysis of Practical RANS Simulations for Spinnaker Aerodynamics, Journal of Wind Engineering and Industrial Aerodynamics,v. 96, pp. 143–165.

M. Lombardi, M. Cremonesi, A. Giampieri, N. Parolini, and A. Quarteroni (2012). A strongly coupled fluid-structure interaction model for wind-sail simulation. In 4th High Performance Yacht Design, pages 212–221, Auckland, New Zealand.

F.R. Menter, M. Kuntz, R. Langtry (2003). Turbulence heat and mass transfer. Ten years Ind. Exp. SST Turbul. Model 4, 625–632.

D. Motta, R. G. J. Flay, P. J. Richards, D. J. Le Pelley, J. Deparday, and P. Bot (2014). Experimental investigation of asymmetric spinnaker aerodynamics using pressure and sail shape measurements. Ocean Engineering, 90:104– 118.

S. Nava, J. Cater, and S. Norris (2017). Large eddy simulation of downwind sailing. In Conference on Innovation in High Performance Sailing Yachts INNOVSAIL 2017, Lorient, France.

H. Renzsch and K. Graf (2010). Fluid-structure interaction simulation of spinnakers - getting close to reality. In The Second International Conference on Innovation in High Performance Sailing Yachts, Lorient, France.

H. Renzsch and K. Graf (2013). An experimental validation case for fluid-structure-interaction simulations of downwind sails. In The 21st Chesapeake Sailing Yacht Symposium, Annapolis, Maryland, USA.

J.B. Souppez, A. Arredondo, I.M. Viola (2019). Recent Advances in Numerical and Experimental Downwind Sail Aerodynamics. Journal of Sailing Technology 4(01): 45-65

D. Trimarchi, M. Vidrascu, D. Taunton, S. Turnock, and D. Chapelle (2013). Wrinkle development analysis in thin saillike structures using MITC shell finite elements. Finite Elements in Analysis and Design, 64:48–64.

I.M. Viola (2009). Downwind sail aerodynamics: A CFD investigation with high grid resolution. Ocean Engineering, 36(12):974–984.

I.M. Viola, S. Bartesaghi, T. Van-Renterghem, and R. Ponzini (2014). Detached Eddy Simulation of a sailing yacht. Ocean Engineering, 90:93–103.

I.M. Viola and R. G. J. Flay (2009). Force and Pressure Investigation of Modern Asymmetric Spinnakers. International Journal of Small Craft Technologie, 151.

I.M. Viola and R. G. J. Flay (2011). Sail pressures from fullscale, wind-tunnel and numerical investigations. Ocean Engineering, 38(16):1733–1743.

I.M. Viola and R. G. J. Flay (2015). Pressure distributions on modern asymmetric spinnakers. International Journal of Small Craft Technology, 152(1):41–48.

I.M. Viola, P. Bot, M. Riotte, (2013). Upwind sail aerodynamics: A RANS numerical investigation validated with wind tunnel pressure measurements, International Journal of Heat and Fluid Flow, (39) 90-101.

S. Wang, J. R. Bell, D. Burton, A. H. Herbst, J. Sheridan and M. C. Thompson (2017). The performance of different turbulence models (URANS, SAS and DES) for predicting high-speed train slipstream. Journal of Wind Engineering and Industrial Aerodynamics, 165, 46-57.

STEP Geometries are available here.